15th International Symposium on Flow Visualization
June 25-28, 2012, Minsk, Belarus

THREE DIMENSIONAL FEATURES IN SWIRLING IMPINGING JETS

A. IANIRO[1,c], D. VIOLATO[2], F. SCARANO[2], G. CARDONE[1]

[1]Dipartimento di Ingegneria Aerospaziale (DIAS), University of Naples Federico II, Naples 80125, Italy
[2]Aerospace Engineering Department, Delft University of Technology, Delft, The Netherlands

[c]Corresponding author: Tel.: +390817683405; Email: andrea.ianiro@unina.it

KEYWORDS:
Main subjects: heat transfer, flow visualization
Fluid: impinging jets, swirl flows
Visualization method: Time-resolved Tomographic PIV
Other keywords: tomography, turbulence

ABSTRACT: The influence of the swirl number on the flow development of a multichannel swirling impinging jet is experimentally analyzed. This investigation is concerned with jets issued from swirling nozzles based on helical inserts, which are easily applicable in an industrial environment. The present investigation is conducted with time-resolved tomographic particle image velocimetry in a water jet facility at a fixed value of the Reynolds number (*Re* equal to 10,000), for five values of the swirl number (*S* equal to 0, 0.2, 0.4, 0.6 and 0.8) and at nozzle-to-plate distance equal to 2 diameters since literature results show an interesting heat transfer behavior for the multichannel swirling impinging jets at low nozzle-to-plate distances. The obtained experimental data (both instantaneous and statistic fields) supply information on the behavior of circular jets, multichannel jets, weak swirl jets and strong swirl jets. Results obtained with swirling impinging jets are also compared with those obtained with a circular impinging jet in the same testing conditions and show that the swirl generator causes the flow at the exit to be divided in four separate jets that produce a flow reversal region in the centre of the jet and four separate impingement regions. Swirling jets are characterized by higher turbulence levels also in the jet core. The swirl causes a broadening of the jet and decreasing arrival speed with increasing swirl number. With reference to the literature, the dependence of heat transfer on the flow field is also described. The instantaneous flow fields show that the circular jet is characterized by the presence of ring vortices that, after impingement, breakup in smaller structures. In particular hairpin-like vortices are seen for distances higher than 2 diameters from the centre of impingement. Swirling jets are characterized by smaller structures both in the outer part of the jet and in the inner flow reversal zone. Those small structures are responsible of turbulence penetration in the jet core and turbulent boundary layer development starting from the jet impingement.

INTRODUCTION. The high heat transfer rate obtainable with impinging jets is well recognized and explained in a wide scientific literature [1,2] and makes the usage of jets very popular in several industrial applications such as paper drying, metal and glass tempering and turbine blades cooling. A huge quantity of data and correlations for heat and mass transfer is available for single, row and multiple jets [3].

The flow topology of circular impinging jets (CJ) is well known [4,5] and is characterized by the nozzle diameter and the nozzle-to-plate distance; it can be mainly subdivided in few characteristic sections: the free jet region, the impingement area, the wall jet area and the entrainment region. The impingement area and the wall jet area are characterized by very different heat transfer rates, therefore one of the main limitations of jet impingement heat transfer is the radial non-uniformity.

For some applications such as electronic cooling or chemical vapor deposition, both high values and radial uniformity of heat and mass transfer are requested. The swirling impinging jet could be a possible solution to achieve a higher heat transfer radial uniformity with respect to CJ. Swirling impinging jets are characterized by tangential velocity components that cause a spiral-shaped motion and the broadening of both the impinged area and the wall jet area; this aspect is also coupled, especially near the stagnation point, with axial flux weakening (Huang and El Genk [6]). The swirl causes the flow to open radially; the spiral effect and the high air velocity on the outer surface of the free jet seem to generate more entrainment than conventional jet. In the central region, toroidal flow reversal zones can be generated in case of high swirl [7]. The impinged area is significantly larger in the swirling jet compared to conventional jet. The

wall jet region essentially coincides with that in the CJ while the entrainment region seems to produce a more pronounced effect.

Several works on the last years focused on the study of swirling impinging jets and flames (see e.g. the very recent works by Ianiro and Cardone [8], Nuntadusit, et al. [9], Nanan et al. [10] and Singh et al. [11]): they show that at small nozzle-to-plate spacings (H/D = 2 and 4), swirling impinging jets give higher heat transfer rate than conventional impinging jets while producing a broadening of the jet. This effect is also in agreement with the recent results by Violato et al. [12] on chevron impinging jets. The high heat transfer enhancement produced by the swirling jets is only partially explained by Ianiro and Cardone [8] with the increasing exit velocity due to the presence of the insert and they say that flow field requires further investigations to be completely understood while, in case of chevron jets, Violato et al. [12] attribute the heat transfer enhancement to a deeper penetration of turbulence in the jet and higher axial velcity of the jet core.

All the flow field studies present in literature deal with flow visualizations or with planar measurements [7]; 3-D measurements can give a better insight with respect to planar measurements as already shown in case of chevron jets by Violato et al. [12] and could be useful for the understanding of the complex behavior of swirling impinging jets.

In this work, swirling impinging jets are investigated by means of time-resolved tomographic PIV [13] at fixed nozzle-to-plate distance and Reynolds number (equal respectively to two diameters and 10,000) and at different Swirl numbers (equal to 0, 0.2 0.4, 0.6 and 0.8). The swirling jets are obtained with helical inserts based on the concept of the cross swirling strips as in [8]. Results obtained with swirling impinging jets are also compared with those obtained with a circular impinging jet in the same testing conditions and, with reference to the literature, is done an attempt to justify the heat transfer characteristics of the swirling impinging jet based on the flow field measurements.

EXPERIMENTAL SETUP. The experimental apparatus for the present study is shown as an assembly sketch in Fig. 1a. It consists of a vertical jet (with a nozzle diameter D equal to 19.7 mm) emerging from the bottom wall of the facility, a large stationary test tank, and impinging on a square Plexiglas target plate (with dimensions of 300x300 mm^2) at a distance of two diameters from the nozzle exit.

The test tank is designed as an octagonal water tank (with a circumscribed diameter of 600 mm and a height of 800 mm) made of Plexiglas allowing full optical access for illumination and tomographic imaging and neutrally buoyant polyamide particles of 56 μm of diameter are employed as seeding particles. The water is recycled to maintain clarity and to save particles; in fact the water exiting the test tank passes directly through a pump, that takes the water from a hole in the bottom of the tank and send it back in the supply line; the flow field is not affected by oscillations caused by the pump. The flow rate $\dot{m}$ is controlled by several valves underneath the test tank and measured by means of a flow meter (a rotameter) located on the supply line before the nozzle. Before the experiments, the water is stored for at least one day in order to reach a uniform temperature.

The basic nozzle subsystem has a straight pipe shape with a convergent connection to the stagnation chamber. The nozzle ends in a sharp exit as a truncated tube as done in many literature experiments (see e.g. [8] and [14]). The two regulating parameters for the experiments performed in this work are the Reynolds number and the Swirl number. The water flow provides a stabilized supply in a range of exit flow rate corresponding to Reynolds numbers ($Re = 4\dot{m}/(\pi\mu D)$) between 500 and 15,000 and the experiments are performed at Reynolds number equal to 10,000. Swirl number is related to the swirl vane angle θ and, according to Gupta et al. [15], is expressed as:

$$S = \frac{2}{3}\left[\frac{1-(d/D)^3}{1-(d/D)^2}\right]\tan\theta \qquad 1$$

where d is the vane pack hub diameter and θ is the swirling angle as shown in Fig. 1b. In the present work, experimental campaigns are performed in order to analyze a non swirling jet (S = 0, also called multichannel jet), weak swirling jets (S = 0.2 and S = 0.4), the condition of transition between weak and strong swirl at S = 0.6 and a strong swirling jet (at S = 0.8). All the results are compared with the reference case of a circular jet without the cross swirling insert.

The illumination is provided by a Quantronix Darwin-Duo Nd-YLF laser (2x 22.5 mJ at 1000 Hz). The laser beam is expanded with two cylindrical lenses to obtain a measurement volume with a thickness of 1.2 D and an area of 5x5 D^2 on the plate surface. The light scattered by the particles is recorded by a tomographic system composed of three Imager pro HS cameras (2016 x 2016 pixels, 11 μm pixel pitch) arranged on the top of the water tank and forming solid angles of 60 degrees, observing the illuminated region through the impinged plate. Nikon objectives of 105 mm focal length are set with a numerical aperture f/# = 22 to allow focused imaging of the illuminated particles. For the chosen

a) b)

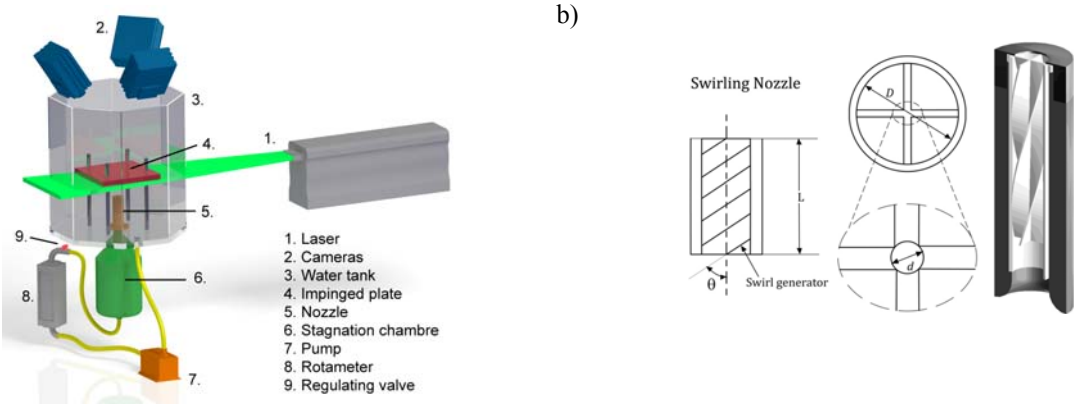

Fig. 1 Experimental apparatus: a) Schematic of the experimental setup b) Schematic of the swirling nozzle

illumination and imaging configuration the particle image density is approximately 0.045 particles/pixel (due to a concentration of 0.48 particles/mm^3).

500 images of tracer particles with a digital resolution of 17.9 pixels/mm are recorded at 500 Hz resulting in high temporal resolution (maximum imaged particle displacement of approximately 25 pixels along the jet axis).

The volumetric light intensity reconstruction is performed with four iterations of the multiplicative algebraic reconstruction technique algorithm applying a pixel to voxel ratio of 1 (the resulting voxel pitch is 53.75 μm) according to Elsinga et al. [13]. The three-dimensional calibration function is corrected by the volume self-calibration to minimize the disparity fields, decreasing in the calibration error from a typical value of 0.3 to 0.03 pixel [16] and the accuracy of the reconstructed object is improved by applying image pre-processing with sliding minimum subtraction over windows of 31x31 pixels.

Three-dimensional particle field motion is computed by volume correlation with a three-dimensional approach corresponding to the approach proposed for two-dimensional images by Astarita [17-18] with a final interrogation volume of 48x48x48 voxels with an overlap between adjacent interrogation boxes of 75%, leading to a vector pitch of 0.0339 *D*. Noisy fluctuations of the velocity vectors are reduced by applying a space-time regression, a second-order polynomial least-square fit over a kernel of 5 points in time and 53 points in space [19] corresponding to a time length of 0.008 s and a volumetric domain of 2.67x2.67x2.67 mm^3. All the measured quantities are presented as non-dimensional: the reference velocity is the average exit velocity and the reference length is the nozzle diameter.

While the errors introduced in the imaging and cross-correlation steps are in common with planar PIV and are estimated to be about 1% of the measured value (see Raffel et al. [20]), the errors coming from the tomographic reconstruction lead to a systematic underestimation of the measured particle displacement gradient magnitude. The measurement precision of three-dimensional three-component measurements can be performed by a-posteriori techniques based on physical criteria. The mass conservation principle can be used to ascertain the consistency of the measured velocity field as also proposed by Zhang et al. [21] and done for tomographic PIV data by Violato et al. [19]. The evaluation of the standard deviation of flow divergence over the entire measurement domain and during the whole observation time yields a statistical estimate of the error associated with the measurement of components of the velocity gradient tensor. Normalizing the error by the typical values measured for the vorticity, a relative error of 4.5% is obtained.

MEASURED QUANTITIES. All the measured quantities are presented as non-dimensional. The reference velocity is the average exit velocity and the reference length is the nozzle diameter.

The averaged flow fields (related to all the considered swirling conditions) are compared in order to analyze the global effect of swirl. The core of the discussion is the analysis of the development of the flow field in the wall jet and in the impingement region. Also flow statistics on turbulent kinetic energy are presented with reference to heat transfer measurements from the literature. Time-resolved Tomo-PIV allows describing accurately the instantaneous flow field and the vortex topology. Instantaneous velocity fields are shown and compared, and the vortical structures are visualized by means of the *Q* criterion [22]. On the basis of these quantitative vortex visualizations, an attempt to define a general vortex topology is done.

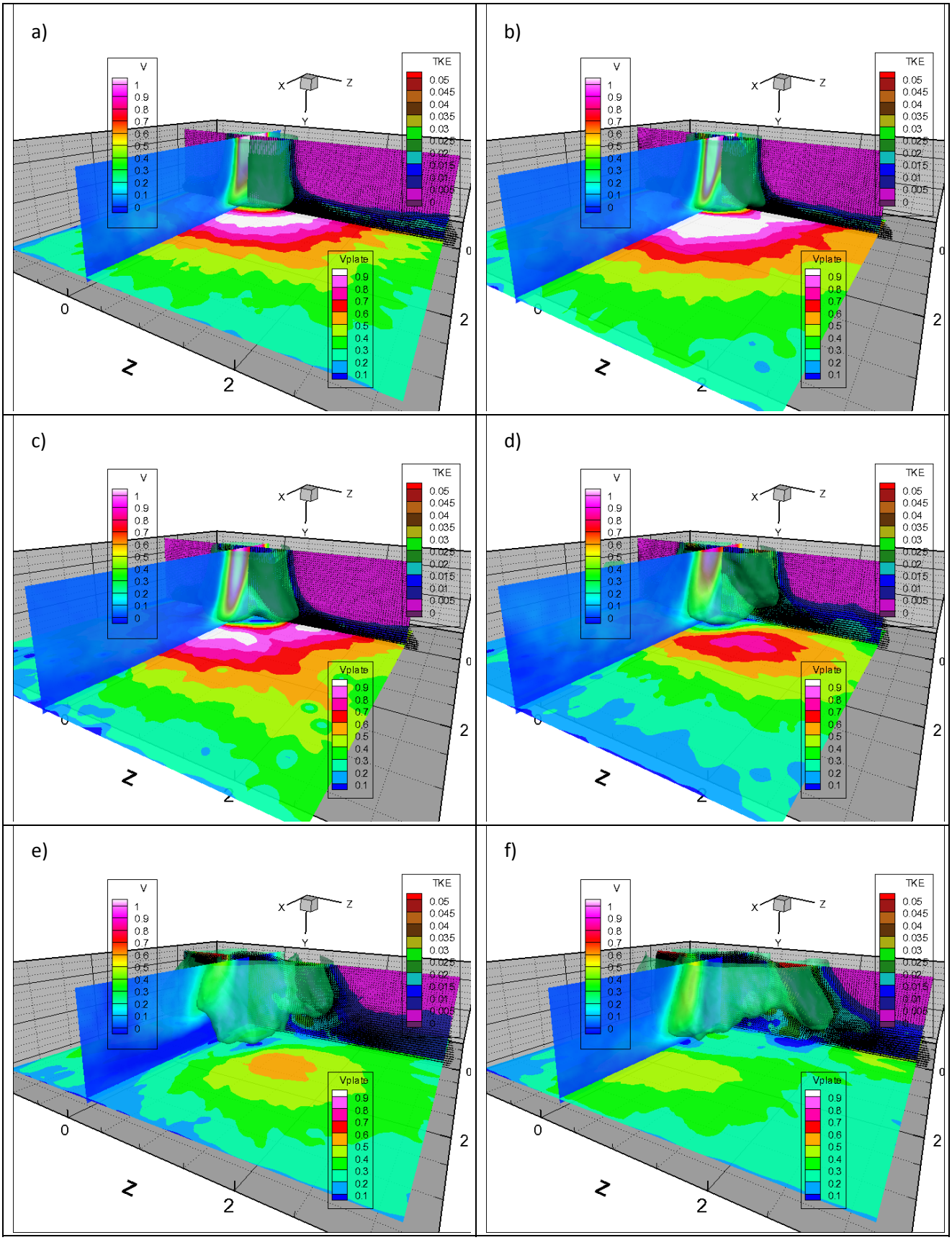

Fig. 2 Flow field statistics - Contour of average velocity nearby the plate, contour of axial velocity on the plane at $Z = 0$, contour of turbulent kinetic energy on the plane at $X = 0$ and isosurface of axial velocity equal to 0.2: a) Circular jet, b) $S = 0$, c) $S = 0.2$, d) $S = 0.4$, e) $S = 0.6$ and f) $S = 0.8$

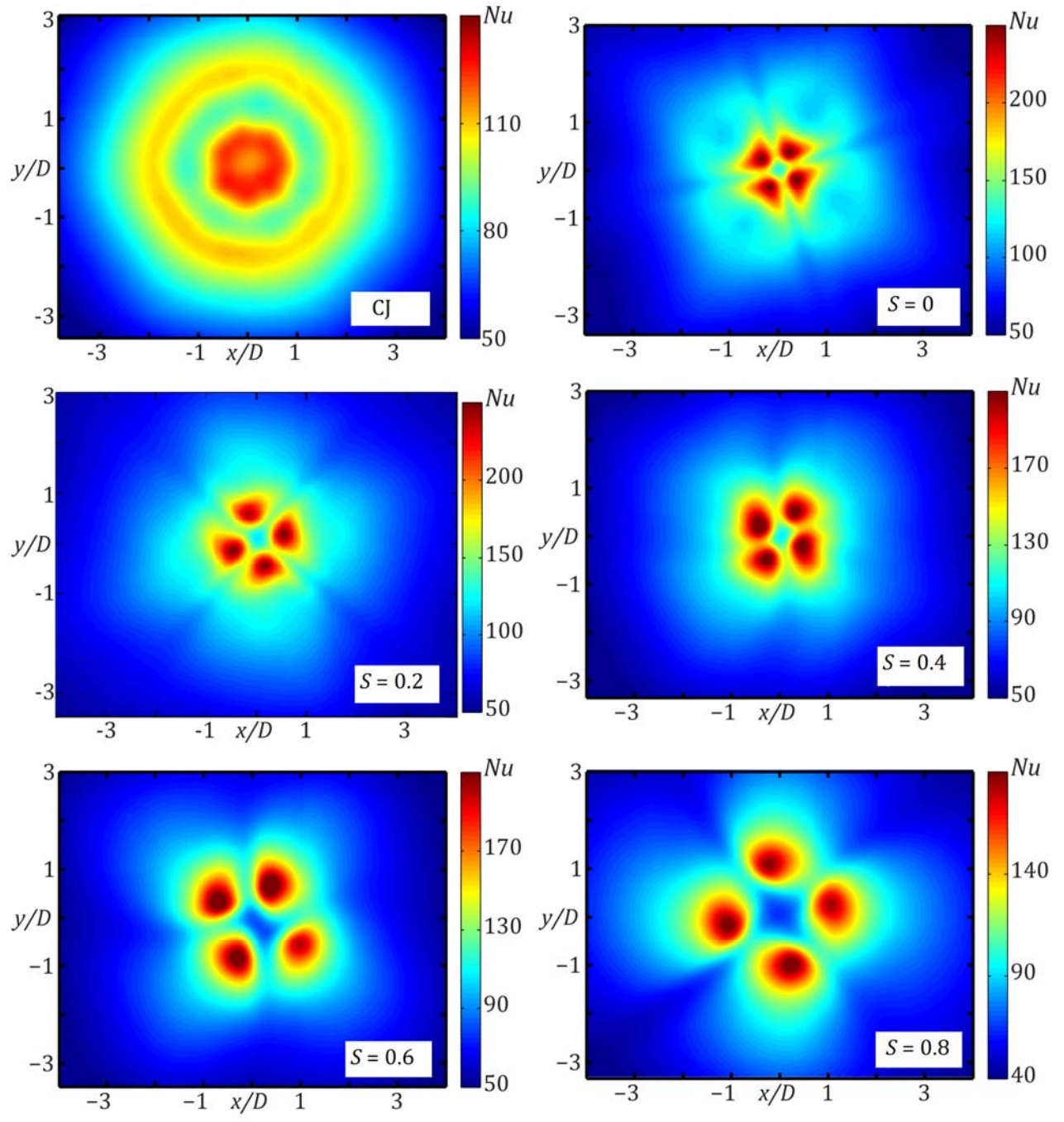

Fig. 3 *Nu* maps for swirling impinging jets at nozzle-to-plate distance equal to two diameters (Adapted from [8])

FLOW FIELD STATISTICS. Flow statistics are presented in Fig. 2 while *Nu* maps obtained by the same nozzles in turbulent conditions at *Re* = 28,000 [8] are presented in figure 3. Despite the fact that the experiments are performed at different Reynolds numbers, both *Re*= 28,000 and *Re* = 10,000 can be considered high enough to have a turbulent jet, thus the average flow features and their influence on the heat transfer can be compared.

In agreement with Glauert [23], on the plate, the circular jet exhibits a stagnation point in the centre if the impingement region, then the flow speed on the plate increases up to at a radial distance of 0.5 diameters from the centre of impingement: this maximum of the velocity on the plate corresponds to the first ring-shaped maximum in Fig 3. After this maximum the velocity decreases and the boundary layer thickness (defined as the height at which wall-parallel flow speed in the wall jet is maximum at a given radial position) increases linearly with the radial distance from the centre of

the impingement. There is also a good correspondence between the location of the second ring-shaped region of maximum in the heat transfer distribution and the peak in near-wall turbulence (as shown also by Narayanan et al. for a slot jet [24]).
All the jets issued by the swirl generator produce higher heat transfer values. This can be explained only partially by a higher arrival speed. In general four jets are issued from the swirling nozzles: the four jets issuing from the pipe do not merge before impinging on the plate and four impingement regions can be identified. Actually the swirling jets are characterized by a region of flow reversal in the centre of the jet and the "four jets" issued from the channels of the swirl generator are strongly deflected before approaching the wall. This results in the formation of localized zones with very high velocities nearby the plate.
Another interesting feature of the swirling jets is the deep penetration of turbulence in the jet core. By inspecting the contours of TKE in Fig. 2, it is evident that the swirling jets already have high levels of turbulent kinetic energy in the jet core in comparison with the circular jet where turbulence is mostly generated in the shear layer and in the wall jet region. The turbulence level on the wall is quite homogeneous and, as in the case of the circular jet, the outer maxima of heat transfer are not expected. The effect of the increasing swirl number is substantially an increase in the size of the jet and subsequently a decrease of the jet arrival speed and an increase of the impinged area (a dramatic reduction of the maximum *Vplate* with the increase of the swirl number is shown in Fig. 2). This explains the displacement from the centre of the impingement and the decrease of the magnitude of the *Nu* peaks (Fig. 3); *Nu* peaks, in fact, correspond to the regions of velocity maxima on the plate shown in Fig. 2. The *Nu* minimum on the centre of impingement corresponds as well to the region flow reversal in the centre of the jet that increases in size with increasing swirl number.

INSTANTANEOUS FLOW FIELDS. The quantitative visualizations of the instantaneous flow field in Fig. 4 and 5 present the contour of axial velocity on the plane at $X = 0$ with velocity vectors on the plane, the contour of velocity on the plate at 0.04 diameters from the plate and the vortex visualization with iso-sourface of $Q = 1.8$ in translucent
The flow field of the circular jet is characterized by the presence of the ring vortices. The velocity vectors show that the fluid coming from the environment joins the jet thanks to the ring vortices that entrain flow from the ambient region and accelerate it on the wall with a pulsatile motion. These vortices are responsible for unsteady flow separation at a radial distance of about 1.5 diameters from the centre of impingement in agreement with the findings of Hadziabdic et al. [25].
On the wall, smaller coherent structures, having the shape of hairpin vortices that are typical of a turbulent boundary layer, are present starting from a distance of about two diameters from the centre of impingement in correspondence of the second ring-shaped region of maximum in the heat transfer distribution and of the peak in near-wall turbulence in Fig. 2 and Fig. 3.
Due to the introduction of the insert, the ring vortices are not visualized in the swirling impinging jets. Turbulence is organized in smaller coherent structures with respect to the case of the circular jet as shown in Fig. 4 for the cases at $S = 0$ and at $S = 0.2$ and in Fig. 5 for the cases at $S = 0.4$, $S = 0.6$ and $S = 0.8$. The swirling jets are characterized both in their external and internal shear layer by small vortices that correspond to the rib vortices visualized in the free swirling jets [26]. Those small coherent structures cause a deeper penetration of turbulence in the core of the jet (Kataoka et al. [27] and by Violato et al. [12]) after the break-up of the vortex rings. Part of the rib-like vortices are elongated in the axial direction, thus producing high entrainment, especially at high swirl while the vortices in the inner part of the jet are responsible of the inner flow reversal.
On the wall, the hairpin vortices develop starting from the region near the impingement and are convected in the wall jet. As expected from the free jet results, with the increase of swirl, the jet broadens in size, a recirculation region develops and arrival speed decreases.

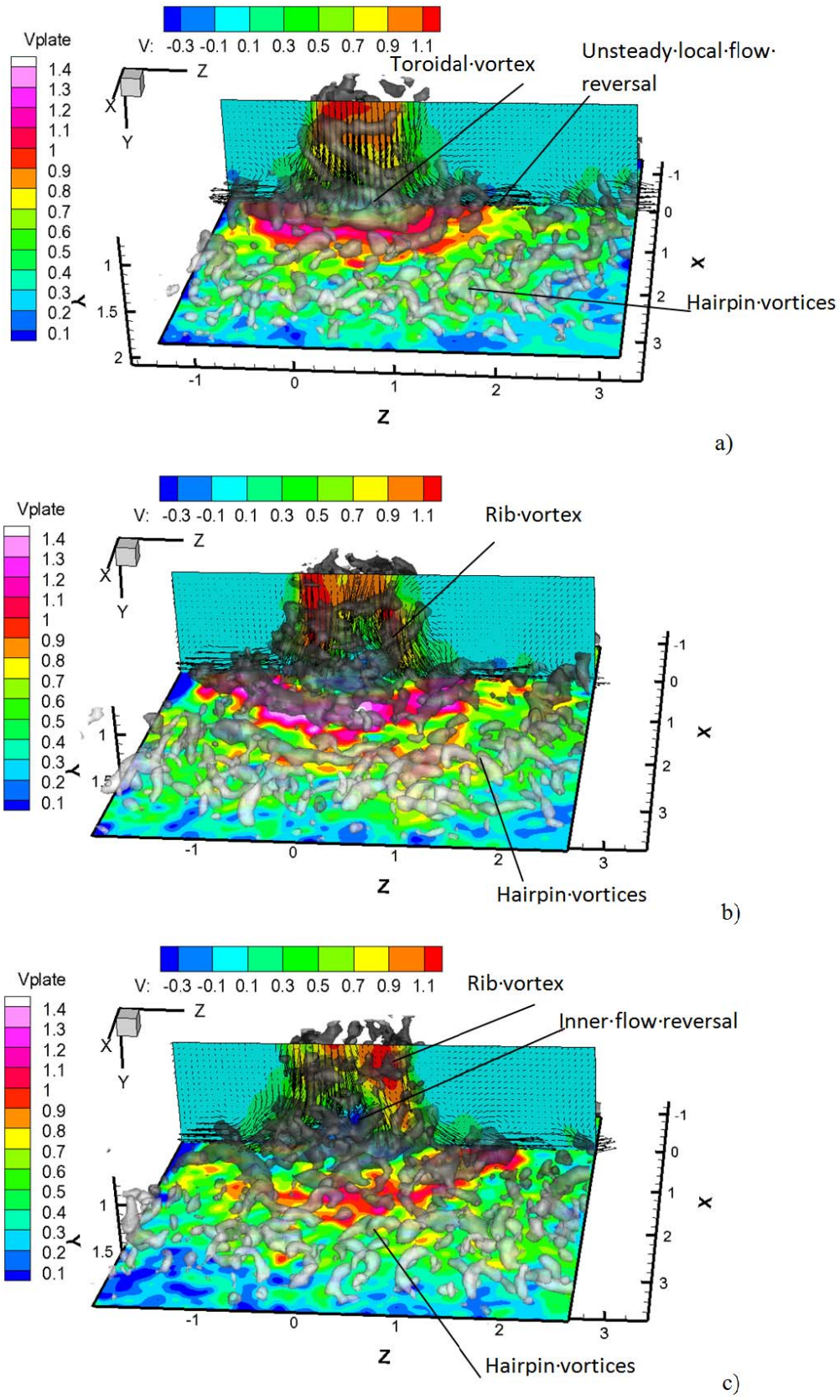

Fig. 4 Instantaneous flow fields - Contour of velocity nearby the plate, contour of axial velocity on the plane at $X = 0$ with vector arrows and isosurface of $Q = 1.8$: a) Circular jet, b) $S = 0$ and c) $S = 0.2$.

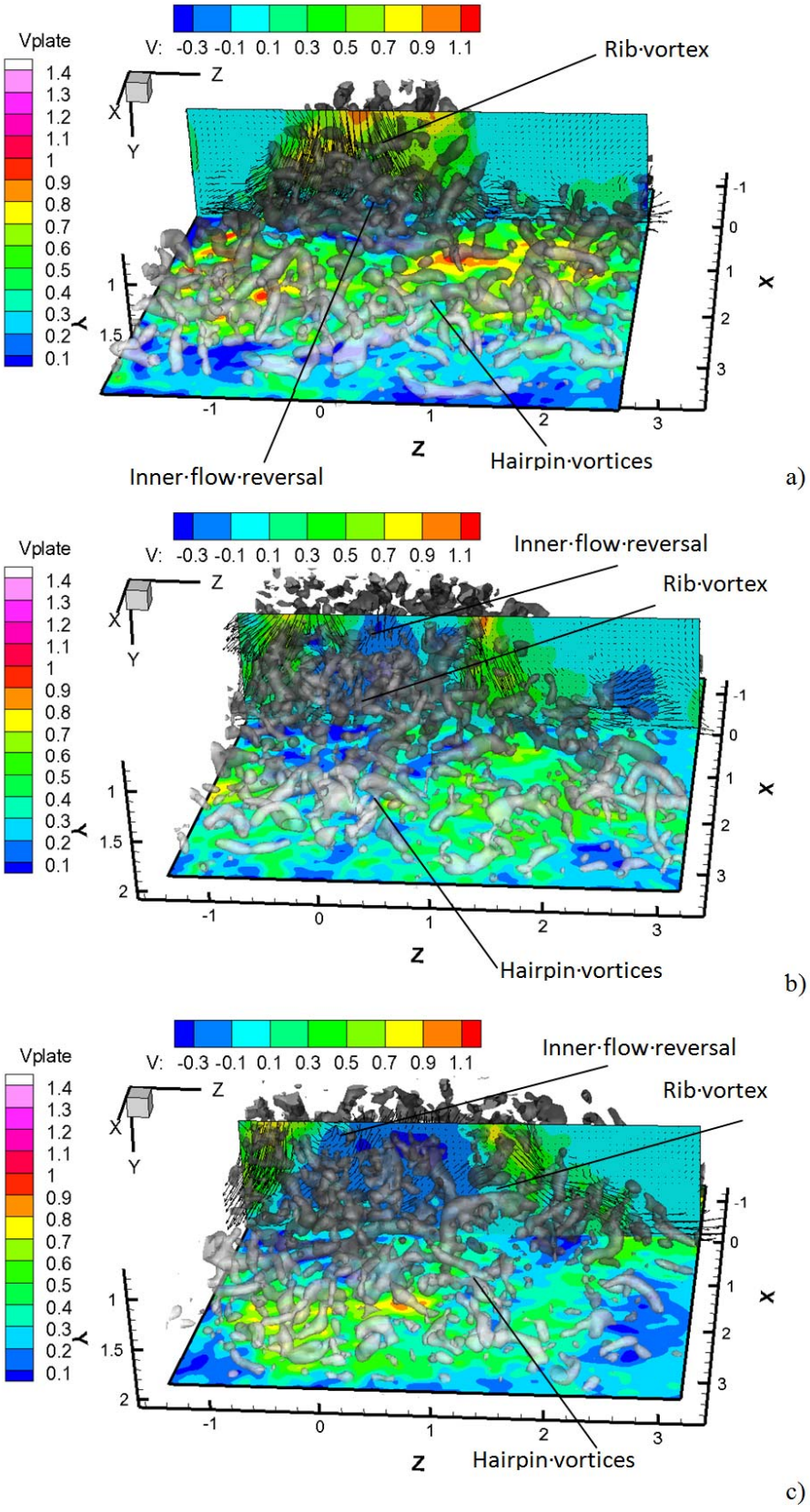

Fig. 5 Instantaneous flow fields - Contour of velocity nearby the plate, contour of axial velocity on the plane at X = 0 with vector arrows and isosurface of $Q = 1.8$: a) $S = 0.4$, b) $S = 0.6$ and c) $S = 0.8$.

CONCLUSIONS. In this work flow field measurements, performed by means of time-resolved Tomo-PIV, are presented for swirling impinging jets, obtained by swirling nozzles with helical inserts. The measured flow fields for different values of the Swirl number are also compared with reference to the flow field of a circular impinging jets. Through the analysis of the flow statistics and instantaneous snapshots, it was possible to quantitatively assess the main features due to the swirl and to the swirl generator.

The swirl generator causes the flow at the exit to be divided in four separate jets that produce a flow reversal region in the centre of the jet and four separate impingement regions. Swirling jets are characterized by higher turbulence levels also in the jet core. The swirl causes a broadening of the jet and decreasing arrival speed with increasing swirl number. With reference to the literature, the dependence of heat transfer on the flow field is also described. The instantaneous flow fields show that the circular jet is characterized by the presence of ring vortices that after impingement breakup in smaller structures, in particular hairpin-like vortices are seen for distances higher than 2 diameters from the centre of impingement. Swirling jets are characterized by smaller structures both in the outer part of the jet and in the inner flow reversal zone. Those small structures are responsible for turbulence penetration in the jet core and turbulent boundary layer development starting from the jet impingement region.

References

1. Martin H. *Heat and Mass Transfer between Impinging Gas Jets and Solid Surfaces.* Advances in Heat Transfer 1977, **13**, p. 1
2. Jambunathan K. et al. *A review of heat transfer data for single circular jet impingement*. International Journal of Heat and Fluid Flow 1992, **13**, p. 106
3. Viskanta R. *Heat Transfer to Impinging Isothermal Gas and Flames Jets.* Experimental Thermal and Fluid Science 1993, **6**, p. 111
4. Gautner J.W. et al. *Survey of Literature of Flow Characteristics of a Single Turbulent Jet Impinging on a Flat Surface* NASA TN D-5652 1970
5. Donaldson C.D. and Snedeker R.S. *A study of free jet impingement. Part 1. Mean properties of free and impinging jets*. J. Fluid Mech. 1971, **45**, p. 281
6. Huang L. and El Genk M.S. *Heat transfer and flow visualization experiments of swirling, multi-channel, and conventional impinging jets*. Int. J. Heat Mass Transfer 1998, **41**, p. 583
7. Alekseenko S.V. et al. *Experimental study of and impinging jets with different swirl rates.* International Journal of Heat and Fluid Flow 2007, **28**, p. 1340
8. Ianiro A. and Cardone G. *Heat transfer rate and uniformity in multichannel swirling impinging jets.* Applied Thermal Engineering 2011, doi:10.1016/j.applthermaleng.2011.10.018
9. C. Nuntadusit, et al. *Visualization of flow and heat transfer characteristics for swirling impinging jet*. Int. Commun. Heat Mass Transf. 2012, doi:10.1016/j.icheatmasstransfer.2012.03.002
10. Nanan K. et al. *Forced convective heat transfer by swirling impinging jets issuing from nozzles equipped with twisted tapes*. Int. Commun. Heat Mass Transf. 2012, doi:10.1016/j.icheatmasstransfer.2012.05.002
11. Singh G. et al. *Heat transfer characteristics of natural gas/air swirling flame impinging on a flat surface.* Experimental Thermal and Fluid Science 2012, **41**, p. 165–176
12. Violato D. et al. *Three-dimensional vortex dynamics and convective heat transfer in circular and chevron impinging jets*. 2012, Under consideration for Int. Journal of Heat and Fluid Flow
13. Elsinga G.E. et al. *Tomographic particle image velocimetry*. Exp Fluids 2006, **41**, p. 933
14. Goldstein R.J. et al. *Streamwise distribution of the recovery factor and the local heat transfer coefficient to an impinging circular air jet.* International Journal of Heat and Mass Transfer 1986, **29**, p. 1227
15. Gupta A.K. et al. *Swirl Flows*. Abacus Press, 1984
16. Wieneke B. *Volume self-calibration for 3D particle image velocimetry*. Exp. Fluids 2008, **45**, p. 549
17. Astarita T. *Analysis of interpolation schemes for image deformation methods in PIV: effect of noise on the accuracy and spatial resolution.* Exp Fluids 2006, **40**, p. 977

18. Astarita T. *Analysis of weighting windows for image deformation methods in PIV*. Exp Fluids 2007, **43**, p. 859
19. Violato D. and Scarano. *Three-dimensional evolution of flow structures in transitional circular and chevron jets*. Physics of Fluids 2011, **23**, 124104
20. Raffel M. et al. *Particle image velocimetry: a practical guide*. 1998, Springer, Berlin Heidelberg New York.
21. Zhang J. et al. *Turbulent flow measurement in a square duct with hybrid holographic PIV*. Exp. Fluids 1997, **23**, p. 373
22. Jeong J. and Hussain F. *On the identification of a vortex*. Journal of Fluid Mechanics 1995, **285**, p. 69
23. Glauert M.B. *The wall jet*. Journal of Fluid Mechanics 1956, **1**, p. 625
24. Narayanan V. et al. *An experimental study of fluid mechanics and heat transfer in and impinging slot jet flow*. International Journal of Heat and Mass Transfer 2004, **47**, p. 1827
25. Ianiro A. *Flow field and heat transfer in swirling impinging jets.* 2011, PhD Thesis, Università degli studi di Napoli Federico II
26. Hadziabdic M. and Hanjalic K. *Vortical structures and heat transfer in a round impinging jet*. Journal of Fluid Mechanics 2008, **596**, p. 221
27. Kataoka K.. et al. *The effect of surface renewal on jet impingement heat transfer*. International Journal of. Heat and Mass Transfer 1987, **30**, p. 559